Electronic Supplementary Material (ESI) for Faraday Discussions.

Supplementary Information for

Probing the Interfacial Structure of Aqueous Surfactants through Helium Atom Evaporation

Xiao-Fei Gao, David J. Hood, Timothy H. Bertram, and Gilbert M. Nathanson*
Department of Chemistry, University of Wisconsin-Madison,
1101 University Avenue, Madison, WI 53706, USA
*E-mail: nathanson@chem.wisc.edu

Table S1. Purities and Concentrations of Chemicals Used in Experiments

Chemicals [a]	Purity
LiBr salt, 6.0 and 8.0 molal	Sigma-Aldrich, ReagentPlus, powder, ≥ 99%
decane, pure	Sigma-Aldrich, ReagentPlus, ≥ 99%
1-butanol, 60 mM	Sigma-Aldrich, anhydrous, 98.5%
3-methyl-1-butanol, 60 mM	Sigma-Aldrich, ACS Reagent, ≥ 98.5%
1-pentanol, 60 mM	Sigma-Aldrich, ACS Reagent, ≥ 98.5%
1-pentanoic acid, 80 and 74 mM	Sigma-Aldrich, ≥ 99%
hexyltrimethylammonium bromide, 100 mM	Sigma-Aldrich, 98%
dodecyltrimethylammonium bromide, 100 mM	Sigma-Aldrich, ≥ 98%
tetrabutylammonium bromide, 50 and 150 mM	Sigma-Aldrich, ACS Reagent, ≥ 98%
benzyltrimethylammonium chloride, 250 mM	Sigma-Aldrich, 97%
48% aqueous HBr enough to lower pH of PA to 3	Sigma-Aldrich, ACS Reagent
lithium hydroxide enough to raise pH of PA to 12	Sigma-Aldrich, powder, ≥ 98%

a. The bulk surfactant concentrations in the 6.0 and 8.0 molal LiBr solutions are accurate to within ± 1 mM for neutral and ± 2 mM for ionic solutes.

Physical Properties of the LiBr/H_2O Solutions

Molalities: 6.0 and 8.0 moles/kg water (molal unit)

Mole ratios: 0.11 and 0.14 LiBr per H_2O

Freezing points: 231 and 210 K for 6.0 and 8.0 m LiBr

Densities: 1.29 and 1.46 g/cm^3 for 6.0 and 8 molal at 290 K

Molarities: 5.1 and 6.7 Molar at 290 K

Viscosities: 6 cP at 255 K and 15 cP at 235 K

Surface tension of bare 6.0 and 8.0 molal LiBr at 290 K: 83 mN/m and 85 mN/m

Table S2. Solution Surface Tension and Microjet Parameters

Surfactant solution	T / K	Surface Tension [a] mN/m	u_{jet} [b] m/s	$L_{breakup}$ [c] mm	P_{vap} [d] torr	λ [e] µm	N_{coll} [f]
5.1 M LiBr/H_2O	255	83	24	6	0.5	700	0.2
60 mM BuOH/5.1 M LiBr/H_2O	255	59	24	7	0.5	700	0.2
60 mM MeBuOH/5.1 M LiBr/H_2O	255	41	24	9	0.5	700	0.2
60 mM POH/5.1 M LiBr/H_2O	255	39	24	9	0.5	700	0.2
80 mM PA/5.1 M LiBr/H_2O	255	41	24	9	0.5	700	0.2
100 mM $HTMA^+$/5.1 M LiBr/H_2O	255	62	24	7	0.5	700	0.2
100 mM $DTMA^+$/5.1 M LiBr/H_2O	255	30	24	11	0.5	700	0.2
74 mM POO^-/5.1 M LiBr/H_2O	255	67	24	6	0.5	700	0.2
250 mM $BTMA^+$/5.1 M LiBr/H_2O	255	57	24	7	0.5	700	0.2
50 mM TBA^+/5.1 M LiBr/H_2O	255	51	24	8	0.5	700	0.2
150 mM TBA^+/5.1 M LiBr/H_2O	255	49	24	8	0.5	700	0.2
5.1 M LiBr/H_2O	235	83	16	5	0.2	1600	0.06
60 mM BuOH/5.1 M LiBr/H_2O	235	59	16	6	0.2	1600	0.07
60 mM MeBuOH/5.1 M LiBr/H_2O	235	41	16	8	0.2	1600	0.07
60 mM POH/5.1 M LiBr/H_2O	235	39	16	8	0.2	1600	0.07
80 mM PA/5.1 M LiBr/H_2O	235	41	16	8	0.2	1600	0.07
250 mM $BTMA^+$/5.1 M LiBr/H_2O	235	57	16	6	0.2	1600	0.07
50 mM TBA^+/5.1 M LiBr/H_2O	235	51	16	7	0.2	1600	0.07
150 mM TBA^+/5.1 M LiBr/H_2O	235	49	16	7	0.2	1600	0.07

74 mM POO^-/5.1 M LiBr/H_2O	235	67	16	6	0.2	1600	0.07
Decane	260	24	24	7	0.06	2240	0.05

a. Surface tensions are measured at 290 K.

b. Microjet speed, as calculated from the 34 μm nozzle diameter and the mass loss of the solution over a specified time.

c. See refs. 1 and 2 for calculating the breakup length $L_{breakup}$ of the cylindrical jet into droplets. The density of the 5.1 M LiBr/H_2O is measured to be 1.29 g/cm^3 at 290 K but less than 0.04 g/cm^3 off from the values at 255 and 235 K.[3] The viscosities of 5.1 M LiBr/H_2O solution are 6 cp and 15 cp at 255 and 235 K, respectively.[3] The density and viscosity of decane are 0.73 g/cm^3 and 1.6 cp at 260 K.[4]

d. The vapor pressures listed are for 5.1 M LiBr/H_2O solution without surfactants. The dilute surfactants should have minimal impact on the water vapor pressure, while they may reduce the evaporative water flux slightly because soluble surfactants do not generally pack tightly enough to impose significant barriers to evaporation.[5]

e. The mean free path λ of collisions between helium atoms and evaporating water molecules is calculated assuming collision cross sections of 15 Å^2 and 40 Å^2 for He-Water and He-Decane collisions. See refs. 1 and 2 for calculations.

f. N_{coll} is the average number of collisions that the helium atom undergoes with evaporating water molecules as it exits the jet and passes through the water vapor cloud. See eq 1 of ref. 2. N_{coll} is smaller at 235 than at 255 K and is lower than 1 in all cases.

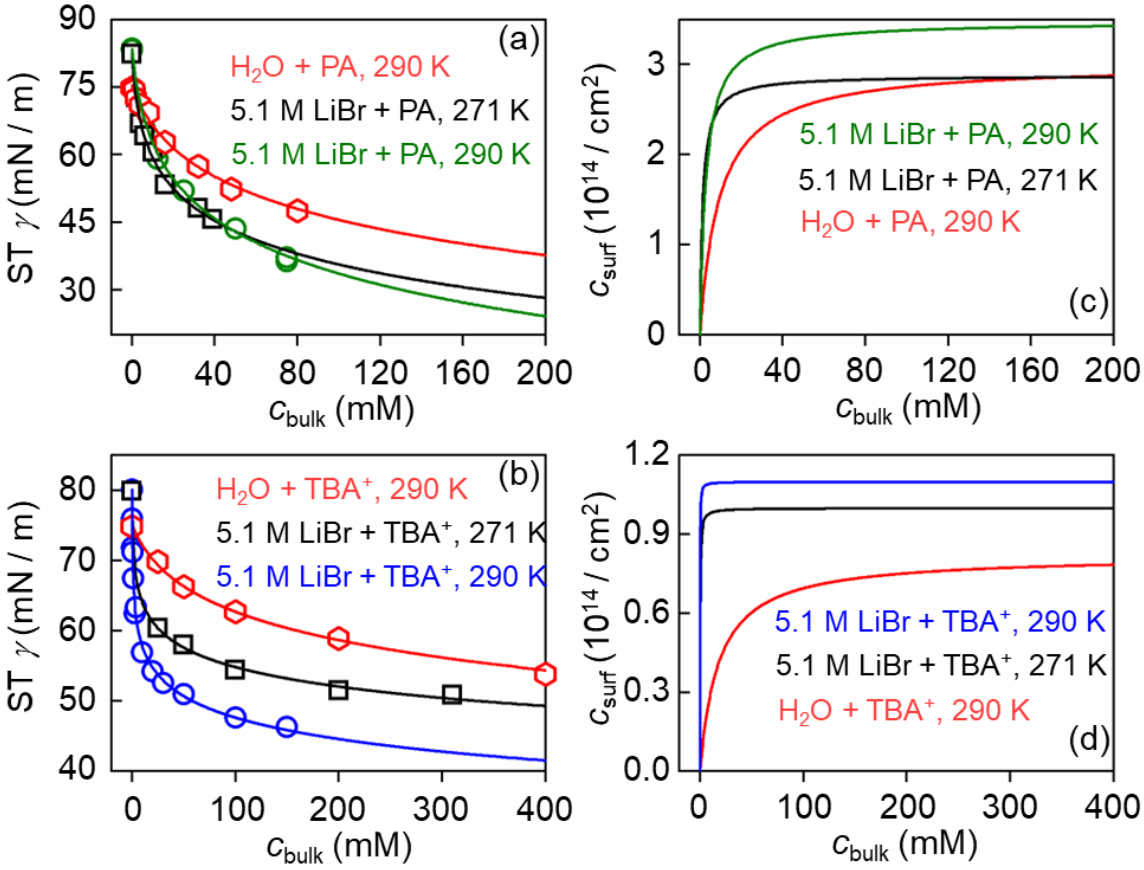

Fig. S1 (a) Surface tensions (ST) γ of 5.1 M LiBr/H_2O + pentanoic acid (PA) at 271 K (black squares) and 290 K (green circles), and pure H_2O + PA (red hexagons) at 290 K as a function of bulk concentration (c_{bulk}) of PA. The solid lines are best-fit curves to the ST data using the three-parameter Szyszkowski equation,[6] $\gamma = \gamma_0 - c_{max}RT\ln(1+K_L*c_{bulk})$, where γ_0, c_{max}, and K_L are the surface tension of the solution at $c_{bulk} = 0$, the maximum surface concentration, and the Langmuir constant. (b) Surface tensions of 5.1 M LiBr/H_2O + tetrabutylammonium (TBA^+) at 271 K (black squares) and 290 K (blue circles), and H_2O + TBA^+ (red hexagon) at 290 K as a function of bulk concentration (c_{bulk}) of TBA^+. The solid lines are best-fit curves to the ST data. The surfactant surface concentrations (c_{surf}) as a function of c_{bulk} are shown in (c) and (d), which correspond to (a) and (b), respectively. c_{surf} and c_{max} are related by the Langmuir equation,

$c_{surf} = c_{max}(K_L c_{bulk})/(1 + K_L c_{bulk})$.

Table S3. Fitting parameters for surfactant surface tension data in 5.1 M LiBr/H_2O [a]

Surfactant solution [b]	γ_0 [c] (mN/m)	c_{max} [d] (1×10^{14} / cm^2)	K_L [d] (M^{-1})	c_{bulk}(max) [e] (mM) at 290 K [240 K]
5.1 M LiBr/H_2O + Neutral Surfactants				
BuOH	85 ± 1	3.4 ± 0.2	100 ± 20	>120 [>120]
MeBuOH	84 ± 1	3.3 ± 0.1	420 ± 45	>100 [>100]
POH	84 ± 1	3.9 ± 0.2	300 ± 36	>300
PA	83 ± 1	3.5 ± 0.1	350 ± 48	>200 [80]
PA (271 K)	82 ± 1	2.9 ± 0.2	750 ± 160	120
5.1 M LiBr/H_2O + ionic Surfactants				
$HTMA^+$	82 ± 1	1.3 ± 0.1	440 ± 120	120 [>100]
TBA^+	83 ± 1	1.1 ± 0.1	21000 ± 5700	>320 [150]
TBA^+ (271 K)	80 ± 1	1.0 ± 0.1	5200 ± 2500	320
$BTMA^+$	84 ± 1	2.8 ± 0.2	37 ± 9	>350 [>250]
$DTMA^+$	83 ± 1	2.4 ± 0.3	8.1×10^5 ± 3.7×10^5	>300 [>100]
POO^-	82 ± 1	2.1 ± 0.3	65 ± 23	>240

a. The surface tension measurements were fit with the Szyszkowski equation, $\gamma = \gamma_0 - c_{max}RT\ln(1+K_L*c_{bulk})$ by allowing three parameters to float: γ_0, c_{max}, and K_L. Most fitted values of γ_0 encompass the actual measured values within the listed error bars.

b. The solution temperature is 290 K if not specified.

c. γ_0 represents the surface tension of the bare 5.1 M LiBr solution without surfactants. Different batches of 5.1 M LiBr/H_2O solutions vary slightly (80 ± 1.5 mN/m) in the surface tensions due to non-identical sources of LiBr salts and surface-suctioning procedures. Each series of surfactant solutions in the surface tension measurements use bare LiBr/H_2O solutions from the same batch, the surface tensions of which are repeatable within ± 1 mN/m from day-to-day tests.

d. The errors represent the fitting error of one standard deviation from a non-linear least squares fit carried out in Python using scipy.optimize.curve_fit.

e. Surfactant solubility was measured in 5.1 M LiBr/H_2O at 290 K, unless otherwise specified. Solubility at 240 K is shown in brackets.

Table S4. Comparison of surface tension fitting parameters with literature [a]

Surfactant solution	c_{max} [b] (1×10^{14} / cm^2) in 5.1 M LiBr/H_2O at 290 K	c_{max} [b] (1×10^{14} / cm^2) in pure H_2O from literature	K_L [b] (M^{-1}) in 5.1 M LiBr/H_2O at 290 K	K_L [b] (M^{-1}) in pure H_2O from literature
5.1 M LiBr/H_2O + Neutral Surfactants				
BuOH	3.4	4.4 (298 K) [7]	99	12 (298 K) [7]
		3.2 (293 K) [8]		23 (293 K) [8]
PA	3.5	3.0 (293 K) [9]	350	91 (293 K) [9]
MeBuOH	3.3	3.9 (293 K) [8]	420	58 (293 K) [8]
POH	3.9	3.5 (293 K) [10]	300	94 (293 K) [10]
		4.2 (298 K) [7]		56 (298 K) [7]
5.1 M LiBr/H_2O + Ionic Surfactants				
$HTMA^+$	1.3	0.84 (298 K) [11]	440	79 (298 K) [11]
		0.96 (298 K) [12]		180 (298 K) [12]
TBA^+	1.1	0.69 (298 K) [13]	16000	72 (298 K) [13]
		0.61 (298 K) [14]		190 (298 K) [14]
$BTMA^+$	2.8	1.8 (303 K) [15]	37	
		2.5 (298 K) [c 16]		60 (298 K) [c 16]
$DTMA^+$	2.4	1.5 (295 K) [17]	810000	910 (295 K) [17]
		1.7 (298 K) [d 18]		3200 (298 K) [d 18]

a. The surface tension measurements were fit with the Szyszkowski equation, $\gamma = \gamma_0 - c_{max}RT\ln(1+K_L*c_{bulk})$ by allowing three parameters to float: γ_0, c_{max}, and K_L.

b. The data were fit using the non-linear least squares method carried out in Python using scipy.optimize.curve_fit.

c. Surface tension data was measured in 6.7 M LiBr/H_2O.

d. Surface tension data was measured in 0.1 M NaBr/H_2O

Table S5. Surfactant Packing Properties at Experimental Bulk Concentrations

Surfactant solution [a]	Surfactant surface concentration (c_{surf}) [b] (1×10^{14} / cm^2)	Limiting molecular [c] area A_{min} (Å^2)	Surface coverage θ = c_{surf}/c_{pack} [c] (from 0 to 1) [d]
5.1 M LiBr/H_2O + Neutral Surfactants			
60 mM BuOH	2.9 ± 0.3	19 [19]	0.55 ± 0.06
60mM MeBuOH	3.1 ± 0.1	24 [20]	0.74 ± 0.02
60 mM POH	3.7 ± 0.2	19 = BuOH	0.70 ± 0.03
80 mM PA	3.4 ± 0.2	22 [21]	0.75 ± 0.04
80 mM PA (273 K)	2.8 ± 0.2	22 [21]	0.62 ± 0.04
5.1 M LiBr/H_2O + Ionic Surfactants			
100 mM $HTMA^+$	1.3 ± 0.1	32 [22]	0.42 ± 0.03
50 mM TBA^+	1.1 ± 0.03	50 [22]	0.55 ± 0.02
150 mM TBA^+	1.1 ± 0.03	50 [22]	0.55 ± 0.02
50 mM TBA^+ (273 K)	1.0 ± 0.07	50 [22]	0.50 ± 0.04
150 mM TBA^+ (273 K)	1.0 ± 0.07	50 [22]	0.50 ± 0.04
250 mM $BTMA^+$	2.5 ± 0.3	32 = $HTMA^+$	0.80 ± 0.08
100 mM $DTMA^+$	2.4 ± 0.3	32 = $HTMA^+$	0.77 ± 0.08
74 mM POO^-	1.7 ± 0.3	22 = PA	0.37 ± 0.06

a. The liquid temperature is 290 K if not specified.

b. The uncertainty in the surface concentration (Δc_{surf}) is calculated from error propagation: $\Delta c_{surf} = \partial c_{surf}/\partial c_{max} * \Delta c_{max} + \partial c_{surf}/\partial K_L * \Delta K_L + \partial c_{surf}/\partial c_{bulk} * \Delta c_{bulk}$, where Δc_{max}, ΔK_L, and Δc_{bulk} are uncertainties in c_{max}, K_L and c_{bulk}. The uncertainties Δc_{max} and ΔK_L are obtained from a least-squares fit of the Szyszkowski equation, while Δc_{bulk} is the error of surfactant bulk concentration in making solutions.

c. The minimum areas are not derived from the fitted values of c_{max}, but rather taken from the specified literature as the smallest measured area. The maximum packing density $c_{pack} = 1/A_{min}$.

d. The uncertainty in the surface coverage ($\Delta\theta$) is calculated from $\Delta\theta = d\theta/dc_{surf} * \Delta c_{surf}$.

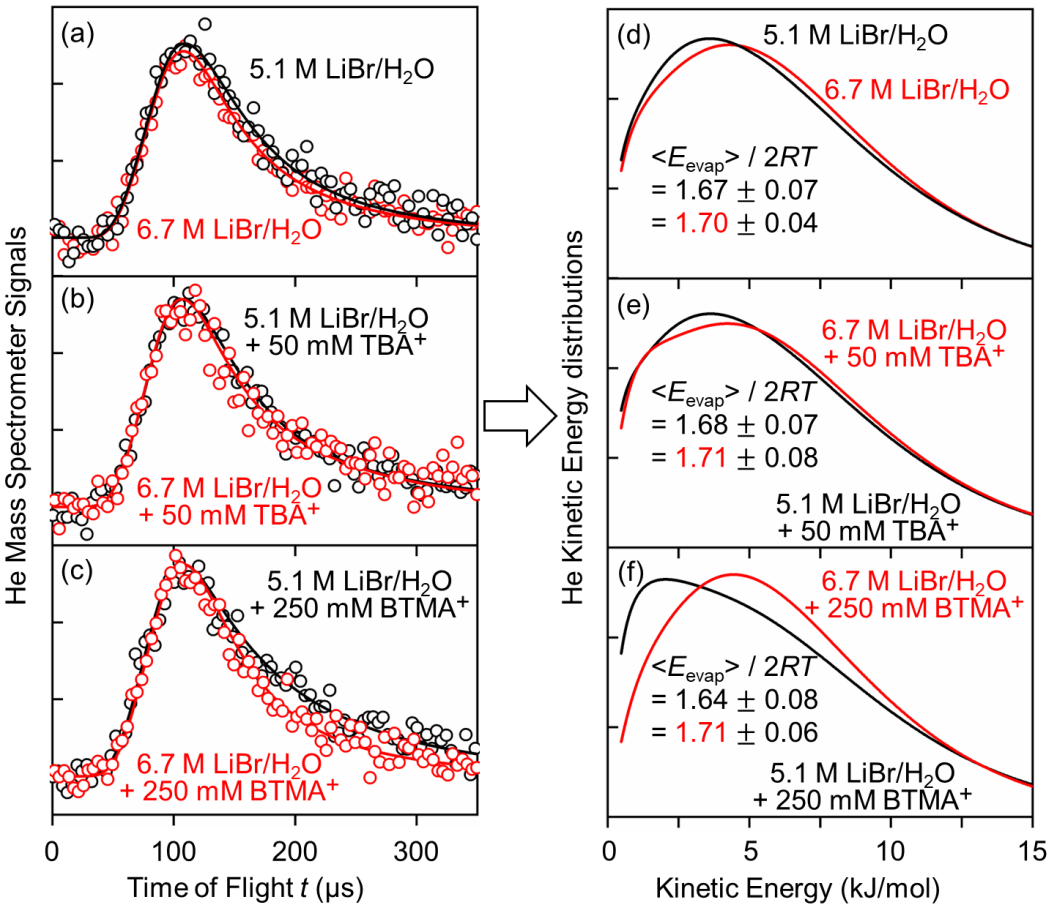

Fig. S2 Time-of-flight spectra (left) and flux-weighted energy distributions (right) of helium atoms evaporating from 5.1 M (6.0 molal) LiBr/H_2O (black) and 6.7 M (8.0 molal) LiBr/H_2O (red) solutions without surfactants (a, d), with 50 mM TBA^+ (b, e), and with 250 mM $BTMA^+$ (c, f) at 235 K. The labels are: TBA^+ = tetrabutylammonium, and $BTMA^+$ = benzyltrimethylammonium. $\langle E_{evap} \rangle / 2RT$ represents the flux-weighted kinetic energy of evaporating He atoms with respect to 2 *RT*, the analogous average energy for a Maxwell-Boltzmann distribution.

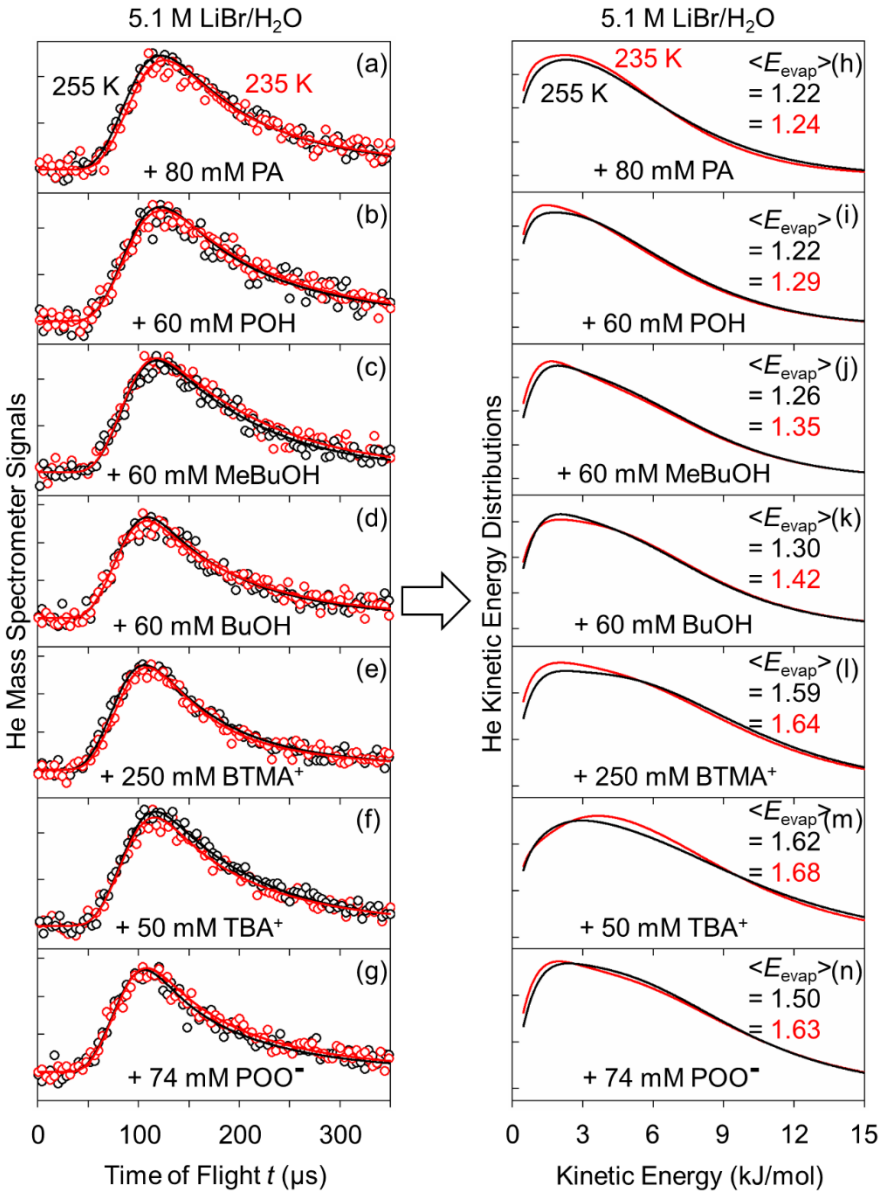

Fig. S3 Time-of-flight spectra (left) and flux-weighted energy distributions (right) of helium atoms evaporating from 5.1 M LiBr/H_2O solutions with added surfactants. Black = 255 K and Red = 235 K. The labels are: PA = pentanoic acid, POH = pentanol, MeBuOH = 3-methyl-1-butanol, $BTMA^+$ = benzyltrimethylammonium, and TBA^+ = tetrabutylammonium. $\langle E_{evap} \rangle$ represents flux-weighted kinetic energy of evaporating He atoms with respect to 2 *RT*. The error bars of $\langle E_{evap} \rangle / 2RT$ vary from ± 0.07 to ± 0.08. Note that the ratios at 255 and 235 K are very similar but systematically higher at lower temperature. This trend has been observed previously in surfactant-free salty water solutions in ref. 23.

Surfactant Adsorption in a Microjet: Helium Evaporation and SF_6 Scattering

We first address the question of how we chose surfactant concentrations for the experiments. The maximum solubilities of the surfactants are listed in the last column of Table S3 (page S5) in comparison with the chosen bulk concentrations in the first column. Pentanol and pentanoic acid are the longest neutral alcohols and carboxylic acids that have > 50 mM solubilities in cold LiBr/H_2O (hexanol solubility is only 12 mM). These concentrations are required for diffusion to significantly populate the surface. The ionic surfactants are more soluble and higher bulk concentrations were selected.

We next discuss the diffusion and adsorption of surfactants to the surface of the fast-flowing microjet. The jet travels a distance of 1.0 mm from the nozzle tip to the center of the observation region in times t = 42 μs at 255 K and 63 μs at 235 K. They are equal to the time for the surfactant to diffuse from the bulk to the surface and coat the LiBr/H_2O solution. These short times may be insufficient for the surfactants to fully coat the surface of the jet. In particular, as surfactant molecules populate the surface region, some diffuse back into solution and some diffuse to the surface but do not stick because the surface site is already filled.[6] These processes slow down the formation of a complete, equilibrium monolayer. Such considerations are particularly important for the ionic surfactants in this study because their high values of $<E_{evap}>/2RT$ might be interpreted to mean that the surfactants did not have sufficient time to segregate to the surface of the microjet.

Numerical methods may be used to estimate the filling time of a monolayer that depend on the surfactant diffusion coefficient and Langmuir constants.[6] These methods depend on the product $(Dt)^{½}$, where D is the surfactant diffusion coefficient. For pentanol, D is 1×10^{-6} and

0.4×10^{-6} cm^2/s at 255 and 235 K in 6.0 molal $LiBr/H_2O$, while for TBA^+, D is 60% of these values.[24] In each case, D is estimated from the value in pure water at 298 K and the Stokes-Einstein equation, $D_2/D_1 = (T_2\,\eta_1)/(T_1\eta_2)$. $(Dt)^{½}$ is roughly the depth over which the surfactant must diffuse to populate the surface, equal to approximately 700 Å at 255 K and 500 Å at 235 K.

We chose not to model segregation because of a lack of surface tension information at 255 or 235 K. Instead, we investigate experimentally the effects of temperature, surfactant concentration, and aging time under actual operating conditions. Fig. S3 (previous page) compares helium evaporation at 255 and 235 K, where the ratio of $(Dt)^{½}$ at 255/235 K is 1.4. The values of $\langle E_{evap}\rangle/2RT$ are up to 11% larger at 235 K than 255 K, which is the same trend observed for helium evaporating from bare $LiBr/H_2O$.[23] The different diffusion depths do not seem to affect $\langle E_{evap}\rangle/2RT$ in an unexpected way, suggesting that the monolayers are fairly well populated at 255 and 235 K.

A more sensitive test can be gleaned from Fig. S4. These panels compare He evaporation from TBA^+ at 255 K at (a) 50 mM and (b) 150 mM bulk concentration, and (c) for a 3.5-fold longer aging time at 150 mM. The values of $\langle E_{evap}\rangle/2RT$ drop 9% from 1.62 to 1.52 to 1.47. This decrease may be correlated with higher surfactant concentrations (see Fig. 8b in the main text). The trend in Fig. S4 implies that TBA^+ populates the surface more densely when the bulk concentration is higher and the aging time is longer, and thus that TBA^+ segregation is not quite complete at the shortest time. Still, $\langle E_{evap}\rangle/2RT$ changes by only 9% and is not close to the 1.19 value for decane.

Lastly, we used high energy SF_6 scattering to determine the presence of one surfactant, TBA^+, at the surface of the microjet and its change in monolayer population with bulk

concentration and aging time. We found previously that the impulsive energy loss of SF_6 molecules upon collision with a liquid depends sensitively on the mass of the surface species when one species is heavy and compact, such as TBA^+.[25] Trends in this energy loss also track changes in equilibrium surface concentrations, as measured by surface tension at room temperature. We therefore use SF_6 scattering here to infer changes in surface segregation.

Fig. S5 compares 300 kJ/mol SF_6 scattering at different TBA^+ concentrations and different distances, *d*, between the nozzle tip and the center of the observation region. This distance is proportional to the aging time.

Panel a contrasts the recoil of SF_6 from bare 5.1 M $LiBr/H_2O$ and a solution containing 50 mM TBABr at 255 K. The scattering is performed at d = 5.3 mm in order to avoid collisions of SF_6 with the tip of the glass nozzle. The SF_6 spectrum shows a distinct peak at short arrival times (high speeds) when TBA^+ is added to solution. This peak corresponds to high recoil energies as the SF_6 molecules scatter from the heavy TBA^+ ions, reflecting their presence in the interfacial region. Panel (b) compares measurements of SF_6 scattering from 50 mM TBA^+ at d = 4.3 and 5.3 mm. The nearly identical spectra show that an increase in aging time from 140 to 220 μs does not alter the surface concentration of TBA^+. Moreover, the 50 mM TBA+ solution at d = 4.3 mm was shown in ref. 25 to create an equilibrium TBA^+ film. Panel c shows SF_6 scattering from a solution of 150 mM TBA^+ and at the same distance d = 3.5 mm used in the helium evaporation spectrum in Fig S4(c). The overlap with the 50 mM solution in panel b indicates that the surface of this solution is also saturated with TBA^+ at its equilibrium value. Thus, we infer that the maximum overshoot of $\langle E_{evap} \rangle / 2RT$ is the 9% value for 50 mM TBA^+ quoted above, which is likely similar for the other ionic surfactants at bulk concentrations greater than 50 mM, as used in this study.

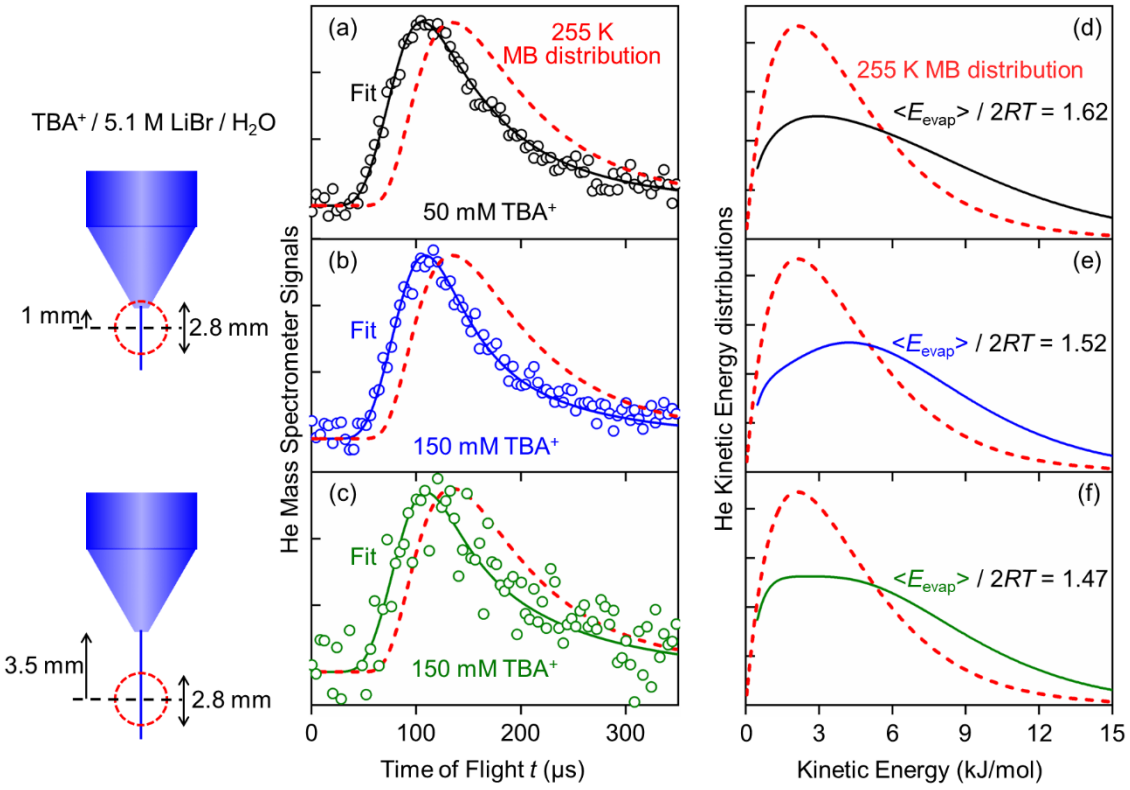

Fig. S4 Time-of-flight spectra (left) and flux-weighted energy distributions (right) of helium atoms evaporating from 5.1 M LiBr/H_2O solutions containing tetrabutylammonium (TBA^+). The TBA^+ bulk concentrations and the distances between the nozzle tip and the center of the viewing region are (a, d) 50 mM and ~ 1 mm, (b, e) 150 mM and ~ 1 mm, and (c, f) 150 mM and ~ 3.5 mm. The viewing region of the detector (dashed circles) is 2.8 mm in diameter. $\langle E_{evap} \rangle / 2RT$ represents flux-weighted kinetic energy of evaporating He atoms with respect to 2 *RT.* The error bars for $\langle E_{evap} \rangle / 2RT$ are ± 0.07 (d), ± 0.07 (e), and ± 0.08 (f). The signal is weaker in panel (c) because helium is highly insoluble in salty water and is rapidly depleted from the near surface region when the jet is exposed to vacuum.

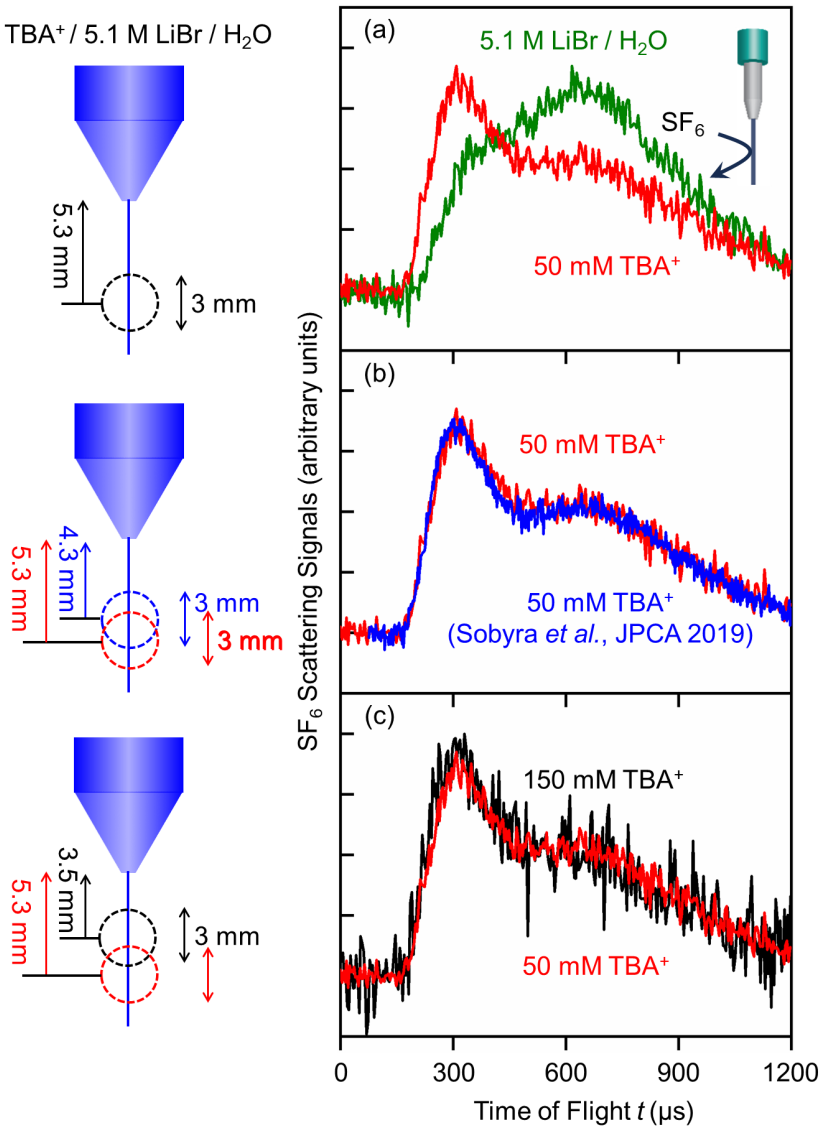

Fig. S5 Time-of-flight spectra of SF_6 scattering from 5.1 M LiBr/H_2O without and with tetrabutylammonium (TBA^+) at different concentrations and aging times. The incident translational energy of the SF_6 molecules is close to 300 kJ/mol. *d* = distance between the nozzle tip and the center of the observation region. (a) comparison of bare and added 50 mM TBA^+ at *d* = 5.3 mm between nozzle and observation region, (b) comparison of 50 mM TBA^+ at *d* = 4.3 and 5.3 mm, (c) comparison of 50 mM TBA^+ at *d* = 5.3 mm and 150 mM TBA^+ at *d* = 3.5 mm. The aging times are 150, 140, and 220 μs for d = 3.5, 4.3, and 5.3 mm. The blue curve is adapted from ref. 25 in which the jet speed is 30 - 32 m/s, higher than 24 m/s in the current experiments.

References

1. J. A. Faust and G. M. Nathanson, *Chem. Soc. Rev.*, 2016, **45**, 3609-3620.
2. X. F. Gao and G. M. Nathanson, *Acc. Chem. Res.*, 2022, **55**, 3294-3302.
3. V. P. Mashovets, N. M. Baron and M. U. Shcherba, *Zh. Prikl. Khim.*, 1971, **44**, 1981-1986.
4. D. R. Caudwell, J. M. Trusler, V. Vesovic and W. A. Wakeham, *J. Chem. Eng. Data*, 2009, **54**, 359-366.
5. G. T. Barnes, *Colloid Surf. A-Physicochem. Eng. Asp.*, 1997, **126**, 149-158.
6. C. H. Chang and E. I. Franses, *Colloid Surf. A-Physicochem. Eng. Asp.*, 1995, **100**, 1-45.
7. K. K. Cheng and C. Park, *Heat Mass Transf.*, 2017, **53**, 2255-2263.
8. C. C. Addison, *J. Chem. Soc.*, 1945, 98-106.
9. F. Suárez and C. M. Romero, *J. Chem. Eng. Data*, 2011, **56**, 1778-1786.
10. C. M. Romero, E. Jiménez and F. Suárez, *J. Chem. Thermodyn.*, 2009, **41**, 513-516.
11. D. Gómez-Díaz, J. M. Navaza and B. Sanjurjo, *J. Chem. Eng. Data*, 2007, **52**, 889-891.
12. J. C. Sanabria and C. M. Romero, *J. Mol. Liq.*, 2022, **366**, 120283.
13. K. Tamaki, *Bull. Chem. Soc. Jpn.*, 1974, **47**, 2764-2767.
14. H. Akiba and R. Ohmura, *J. Chem. Thermodyn.*, 2016, **92**, 72-75.
15. Y. H. Gao, J. L. Chai, J. Xu, G. Z. Li and G. Y. Zhang, *J. Dispersion Sci. Technol.*, 2006, **27**, 1059-1063.
16. X. F. Gao, D. J. Hood, X. Y. Zhao and G. M. Nathanson, *J. Am. Chem. Soc.*, 2023, **145**, 10987-10990.
17. C. Kotsmar, E. V. Aksenenko, V. B. Fainerman, V. Pradines, J. Krägel and R. Miller, *Colloid Surf. A-Physicochem. Eng. Asp.*, 2010, **354**, 210-217.

18. P. X. Li, R. K. Thomas and J. Penfold, *Langmuir*, 2014, **30**, 6739-6747.

19. L. M. Cosman and A. K. Bertram, *J. Phys. Chem. A*, 2008, **112**, 4625-4635.

20. D. Vollhardt, G. Emrich, S. Siegel and R. Rudert, *Langmuir*, 2002, **18**, 6571-6577.

21. K. Lunkenheimer, W. Barzyk, R. Hirte and R. Rudert, *Langmuir*, 2003, **19**, 6140-6150.

22. G. Para, A. Hamerska-Dudra, K. A. Wilk and P. Warszynski, *Colloid Surf. A-Physicochem. Eng. Asp.*, 2010, **365**, 215-221.

23. C. Hahn, Z. R. Kann, J. A. Faust, J. L. Skinner and G. M. Nathanson, *J. Chem. Phys.*, 2016, **144**.

24. W. M. Haynes, in *CRC Handbook of Chemistry and Physics, Section 5: Ionic conductivity and diffusion at infinite dilution*, ed. J. R. Rumble, CRC press, 104 edn., 2014, ch. 9, pp. 77-79.

25. T. B. Sobyra, H. Pliszka, T. H. Bertram and G. M. Nathanson, *J. Phys. Chem. A*, 2019, **123**, 8942-8953.